7th International Conference on Debris-Flow Hazards Mitigation

Small scale debris-flow experiments on run-up height

Dieter Rickenmann [a,*], Tobias Karrer [a,b], Brian McArdell [a], Christian Scheidl [c]

[a] *Swiss Federal Research Institute WSL, Zuercherstrasse 111, Birmensdorf CH-8903, Switzerland*
[b] *IUB Engineering AG, Heinrichstrasse 147, Zürich CH-8005, Switzerland*
[c] *University of Natural Resources and Life Sciences, Vienna A-1190, Austria*

Abstract

We studied the run-up behavior of debris flows in a small-scale experimental flume using various material compositions, approach flow velocities, and geometries of the obstacle. The experiments were performed with a straight and 4 m to 6 m long flume channel with a circular cross-section of 15 cm top width. The debris flows were released from a head tank. We used three debris-flow mixtures, three channel slopes and either a vertical wall or an adverse slope of 30° as an obstacle. Additional tests were performed using water without sediment. The inclined channel was followed by a 30 cm long horizontal transition reach. Immediately upstream and along this reach we measured the shape of the approaching debris-flow surge with four laser sensors, and determined also the approach flow velocity and depth. The run-up conditions were recorded with a high-speed video camera. The measured run-up conditions were compared with four different theoretical models. The observed run-up conditions differed to some extent between debris-flow mixtures and clear water flows, and there were also some differenced among the debris flow mixtures depending on the relative proportion of coarse particles. The observed run-up heights were generally within the range predicted by the theoretical models, but none of them appears to be universally applicable to the entire range of investigated flow conditions. The commonly used energy principle is not always a conservative method to estimate run-up heights, as has been reported in previous studies.

Keywords: debris flow; experiment; run-up height; flow velocity

1. Introduction and theoretical models

Debris-flow run-up on obstacles in their path has a great practical relevance. For a number of applications the flow velocity of a debris flow is one of the key parameters. Owing to the extreme nature of this process, direct measurements in the field are challenging. One important problem in engineering practice is the estimation of run-up height of debris flows against obstacles in their paths. If no direct measurements are possible, characteristics of debris flow events can be estimated based on post-event field investigations (Scheidl et al., 2015). In the specific case of velocity estimation such field investigations can be based on geological deposits on banks (Scheidl et al., 2015) and flow marks on trees, rocks or walls. In bigger events run-up trimlines at adverse slopes can be used. These post facto estimates of debris flow speeds are only useful, if the models that relate flow speeds to run-up heights are well-founded (Iverson et al., 2016). Unfortunately this is not always the case.

The goal of this study is to systematically investigate the run-up height on obstacles and find a relation to debris-flow parameters. To reach this goal several small-scale laboratory experiments were conducted. The debris-flow velocities as well as the run-up heights were measured independently. The measured flow properties of the incoming flow were used as input to theoretical models, and the predicted run-up heights were then compared with the measured run-up heights.

The (frictionless) Point Mass (PM) model, based on the energy principle and a complete conversion of kinetic energy into potential energy, is the most commonly used to predict debris-flow run-up height against vertical walls

* Corresponding author e-mail address*: dieter.rickenmann@wsl.ch*

(Kwan, 2012; Choi et al., 2015). The PM model used here is formulated for a fluid element moving on top (at the surface) of the approach flow to the obstacle. We note that Iverson et al. (2016) used a modified version of the PM model without adding the approach flow depth h_1 to the final run-up height H. The frictionless Finite Mass (FM) Modell is derived by a mechanical energy balance for a finite mass, as presented by Iverson et al. (2016). Also here, a complete conversion of kinetic energy into potential energy is assumed, but the model is formulated with respect to the center of the finite mass, and a uniform vertical distribution of the mass in its final position (at the vertical wall) is assumed.

Theoretical runout models for mass flows against obstacles (dams) with adverse slopes were developed for snow avalanches, debris flows, and rapid landslides (e.g., Takahashi and Yoshida, 1979; Mancarella and Hungr, 2010), and this model was called Smooth Momentum Flux (SMF) model. So far the SMF model was always formulated and tested on obstacles perpendicular to an inclined channel. Iverson et al. (2016) modified the SMF equation in three key aspects. First, it is assumed that all incoming flow momentum is redirected upslope by centripetal forces that act on the foot of the adverse slope. Second, the focus is on basal flow resistance caused exclusively by Coulomb friction. Third, a more precise treatment of the effects of longitudinal pressure gradients is considered.

One significant recognition from recent research is that the behavior of avalanches impacting a dam can be characterized by shock waves. This approach was first described by Hákonardóttir et al. (2003) and tested for avalanches, steady water flows and granular flows. It was again reported in Jóhannesson et al. (2009) (avalanches) and by Choi et al. (2015), who investigated the run-up mechanism for pure water and supercritical sand flows. Here a generalized version of the Momentum Jump (MJ) approach proposed by Iverson et al. (2016) is used, which accounts for the possibility of non-hydrostatic longitudinal normal stresses and/or a jump in the flow bulk density from upstream to downstream of the jump.

The four theoretical models are summarized in the Table 1 below, where the run-up height H (presented in non-dimensional form as H/h_1) is given as a function of the approach flow depth h_1 and approach flow velocity v_1 and further parameters for. These are g = gravitational acceleration, $Fr_1 = v_1/(gh_1)^{0.5}$ = Froude number (of the approach flow), κ = earth pressure coefficient, θ = angle of adverse slope, and ϕ_e = basal friction angle. Iverson et al. (2016) noted that the MJ Model (Table 1) can be rearranged with the only dependent variable (H/h_1) in the form of a cubic equation.

Table 1. Four theoretical run-up height models that were used for comparison with the experimental results. The models are as presented in Iverson et al. (2016), except for the PM model for which we added the approach flow depth h_1 to obtain the final run-up height H. For the FM, SMF, and MJ models, equal densities $\rho_1 = \rho_2$ are assumed, where ρ_1 refers to the density of the flow before the obstacle and ρ_2 to that in the run-out or run-up zone.

Model equation	*Model name*	*Short name*
$\frac{H}{h_1} = 1 + \frac{v_1^2}{2gh_1} = 1 + \frac{Fr_1^2}{2}$	Point Mass	PM
$\frac{H}{h_1} = 1 + \frac{v_1^2}{gh_1} = 1 + Fr_1^2$	Finite Mass	FM
$\frac{H}{h_1} = \frac{\left(Fr_1 + \frac{\kappa}{2}\frac{1}{Fr_1}\cos^3\theta\right)^2}{\left(1 + \frac{\tan\phi_e}{\tan\theta}\right)}$	Smooth Momentum Flux	SMF
$\frac{H}{v_1^2/g} = \frac{2}{\kappa}\left(\frac{H/h_1}{(H/h_1)^2 - 1}\right) + \frac{1}{Fr_1^2}$	Momentum Jump	MJ

There are two important limitations associated with our study presented here. First, the experiments were performed at a very small scale, which makes it difficult to compare them with natural debris flows (Iverson, 2015). Second, the analytical models considered in Table 1 are based on the assumption of steady, uniform incoming flow;

this has to be kept in mind for our comparison of the experimental observations with the analytical model predictions.

2. Experiments and measurements

The experiments were conducted at the Swiss Federal Institute for Forest, Snow and Landscape Research WSL in Birmensdorf. A schematic overview of the flume and the instrumentation layout is presented in Fig. 1. The flow is started from a reservoir with a gate which can be rapidly opened to initiate a dam-break-like release of the sediment mixture. The reservoir empties into a 60 cm long acceleration section, in which the rectangular cross section smoothly transitions to a semi-circular cross section of the main flume. This main part of length L (s. also below) consists of a flexible plastic half-pipe with a diameter of 0.17 m mounted on a wooden supporting construction and aligned with wooden retaining walls alongside of the plastic half-pipe. The surface of the flume is covered with 40-grid aluminum oxide carbide sandpaper (P40, 1960 siarexx) providing a uniform basal friction layer. At the downstream end the flume bed begins to flatten. In this bend section, 0.22 m long, the flume bed is covered with duct tape (tesa®extra Power Universal) in order to minimize the hydraulic energy losses. The transition from a uniformly sloped, semicircular channel to a horizontal, rectangular outlet does not follow a well-defined geometrical shape but great care was taken to establish a smooth changeover. The flume ends on a planar formwork panel. Vertically placed acrylic sidewalls channel the debris flows on the flat runout surface, 0.24 m long, and help them maintain high speeds as they cross the horizontal runout surface and encounter obstacles. Two geometries of obstacles were used: an adverse slope inclined at 30°, and a vertical wall (inclined at 90°), and both obstacles were 0.8 m wide. In every case there was a gap of 0.05 m in flow direction between the acrylic sidewalls and the beginning of the obstacle. Three different channel inclinations were used to vary the approach flow velocity v_1 in front of the obstacle: 20° and 25° with a flume length L = 6 m, and 40° with L = 4 m.

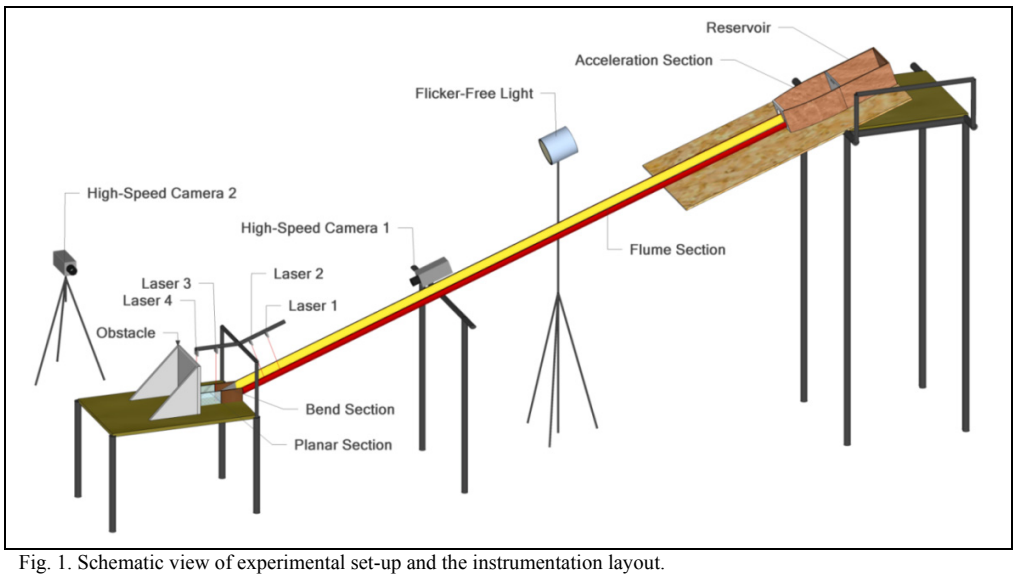

Fig. 1. Schematic view of experimental set-up and the instrumentation layout.

Three sediment-water mixtures with different grain size distribution were used. The experimental mixtures used in this study (A, B and C) are similar to those described in Scheidl et al. (2015) and fit in the large variability of grain size distributions of field debris-flow samples. Scheidl et al. (2015) and Scheidl et al. (2013) provide a comparison between mixtures A, B, C and sediment mixtures used in other studies. The mixtures are based on combinations of loam, crushed stone and water. Four different crushed stone fractions from the KIBAG Kies Stadel AG (Windlach, Switzerland) were used. The loam was imported from the clay pit of Stoob (Austria), a village well known for pottery art. The result of a mineral analysis revealed, that the loam consists of 26 % clay, 60 % silt and 14 % sand. Further the analysis showed that the clay fraction of the loam (< 2µm) contains 22 % illite, 24 % kaolinite and 53 % smectite. Smectite is a swellable clay mineral, which counteracts phase separation for a longer time period

(Scheidl et al., 2013). The mass contribution of each grain size fraction and of the water is given in Table 2. The total weight of each experimental mixture was kept constant at 12 kg. All the mixtures were composed of 60 volume-percent (vol.%) or 73 weight-percent (wt.%) of sediment (loam and crushed stone) and 40 vol.% of (or 27 wt.%) of water. This results in a total volume of approximately 8.1 dm^3 experimental debris flow mass with a bulk density of ρ_{df} = 1484 kg/m^3. The characteristics of the experimental debris mixtures are given in Table 3 which includes also information on the grain size distributions.

The instrumentation layout includes four laser devices at the lower end of the channel to determine flow depth and front velocity. They were mounted directly above the channel with the same inclination as the channel (Fig. 1). Two high speed cameras (monochrome, 800 x 600 pixels, up to 500 frames per second) were mounted to capture the run-up process. One was installed at the side, perpendicular to the flow axis, and the other one captured a frontal view of the run-up. They were triggered with a capacitive proximity switch at the gate in the moment of the gate opening. The lasers recorded flow depths over a time interval of 20 s with an additional pre-trigger of 1 s. The raw data contained a lot of noise and scattered signal due to the wet surface of the channel and the debris flow. For that reason, all raw data was initially filtered. A moving median filter based on a running window of 80 points removed random effects and the signal noise. The measurement frequency of the laser devices is 2 kHz, hence a moving median over 80 points basically averages measurements over a time duration of 1/25 s. The laser devices were calibrated at the beginning of each day. The flow observed at the section of laser 4 was sometimes already influenced by the run-up process ca. 5.5 cm downstream. Some further pre-processing of the laser data was needed to find a robust method to determine reliable values of flow depth and flow velocity before the impact of the flow with the obstacle. If possible the flow depth measured by laser 4 was used as input parameter h_1 for the theoretical models, otherwise the flow depth measured by laser 3 was used as input parameter h_1. The approach flow velocity was determined from the time difference of characteristic positions of the front between two laser cross-sections close to the obstacle.

Table 2. Proportions of the crushed particle fractions used to prepare the sediment mixtures (s. also Table 3).

			Crushed stone fraction			
Mixture	Water [kg]	Loam [kg]	0-2 mm [kg]	2-4 mm [kg]	4-8 mm [kg]	8-11 mm [kg]
A	3.20	2.52	2.52	2.00	0.88	0.88
B	3.20	2.21	2.21	1.75	1.32	1.32
C	3.20	1.89	1.89	1.50	1.76	1.76

Table 3. Characteristics of sediment mixtures used for the experiments. d_{xx} is the sediment particle diameter for which xx% of the mass of is finer. (The mixtures are similar as those used by Scheidl et al., 2015).

Mixture	d_{30} [mm]	d_{50} [mm]	d_{90} [mm]	W [vol.%]	ρ_{df} [kg/m^3]	Total mass [kg]
A	0.1	0.8	4.9	40	1484	12
B	0.2	1.2	5.9	40	1484	12
C	0.4	1.8	6.9	40	1484	12

3. Results and discussion

3.1. Run-up against adverse slope

The normalized run-up heights H/h_1 are shown as a function of the approach flow Froude number Fr_1 in Fig. 2 for the experiments with a 30° adverse slope. Also shown are the normalized run-up heights predicted by the four models listed in Table 1 (whereby the MJ Model equation was solved for the dependent variable H/h_1). We cannot observe a clear stratification of the experimental data, except for a slight tendency of mixture A with the finest sediment to plot at the lower range of the data (for a given Froude number). The FM model provides the most conservative estimate of run-up height (upper bound of theoretical models) for values of Fr_1 larger than 2, and all

experiments resulted in run-up heights smaller than predicted by this model. If the MJ model is assumed to be valid for the experiments, then different earth pressure coefficients κ would be required for different ranges of the Froude number Fr_1 for a best fit with the data, with an approximate value of $\kappa \approx 1.0$ for Fr_1 smaller than about 2.8, and $\kappa \approx 0.4$ for Fr_1 larger than about 2.8 (Fig. 2). The SMF model (which may be appropriate for the run-up against an inclined obstacle) approximately fits the experiments for $\kappa \approx 1.0$ and a basal friction angle ϕ_e between 30° and 40° in the case of Fr_1 larger than about 3, and for $\kappa \approx 1.0$ and $\phi_e \approx 10°$ in the case of Fr_1 smaller than about 3. For comparison, the results from the water experiments are included in a separate plot (inset in Fig. 2); these data are in reasonable agreement with the PM model.

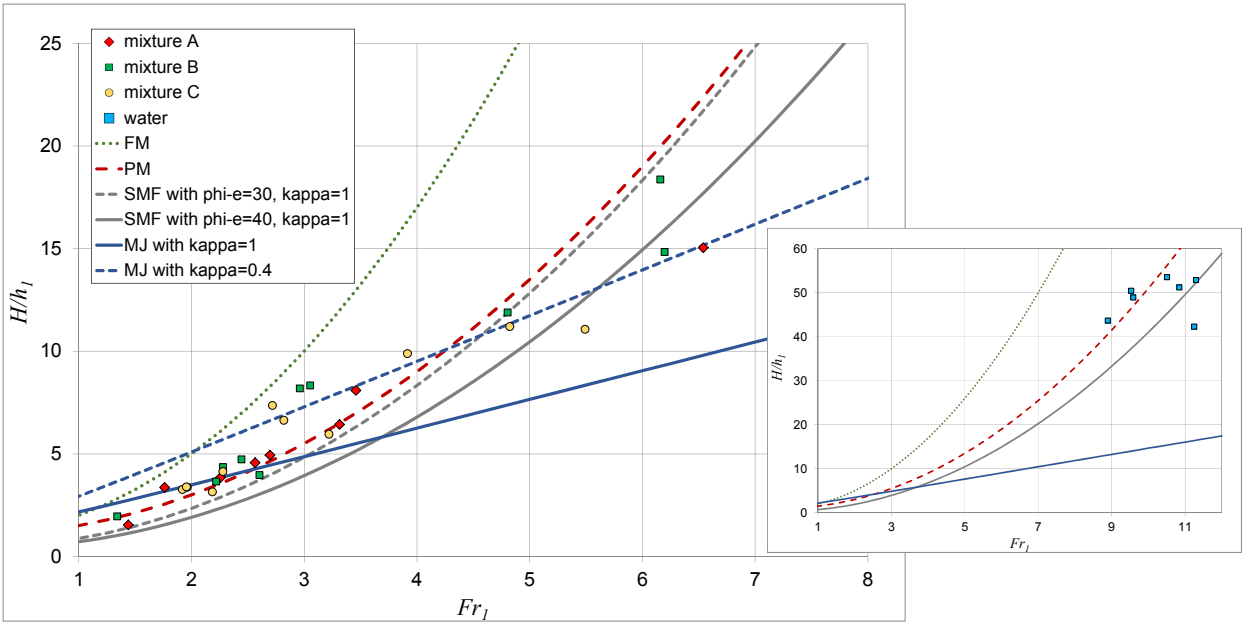

Fig. 2. Run-up heights against an inclined wall (adverse slope of 30°), comparison of experimental results with theoretical models. For the FM, SMF and MJ models equal densities $\rho_1 = \rho_2$ are assumed before and at the obstacle. The inset shows results for the clear water experiments.

3.2. Run-up against vertical wall

For the experiments with a vertical wall as obstacle (i.e. a 90° adverse slope), the normalized run-up heights H/h_1 are shown as a function of the approach flow Froude number Fr_1 in Fig. 3 Also shown are the normalized run-up heights predicted by the four models listed in Table 1 (whereby the MJ Model equation was solved for the dependent variable H/h_1). Again, we cannot observe a clear stratification of the experimental data; in this case, however, there is again a tendency of mixture A with the finest sediment to plot at the lower range of the data for Fr_1 smaller than about 4, whereas the mixture A data tend to plot at the upper range of the data for Fr_1 between 6 and 8. Both the FM and the SMF models (SMF with $\kappa = 1.0$ and $\phi_e = 40°$) appear to provide the most conservative estimate of run-up height (upper bound of theoretical models) for values of Fr_1 larger than about 2, and are closer to the experimental data only for values of Fr_1 between about 1 and 3. The MJ model (which may be appropriate for the run-up against a vertical wall) provides a reasonable fit to the experiments for $\kappa \approx 1.0$ and Fr_1 smaller than about 2.4, and for $\kappa \approx 0.5$ and Fr_1 larger than about 2.4. For comparison, the results from the water experiments are included also here in a separate plot (inset in Fig. 3); in this case the PM model appears to provide an upper limit for the water data.

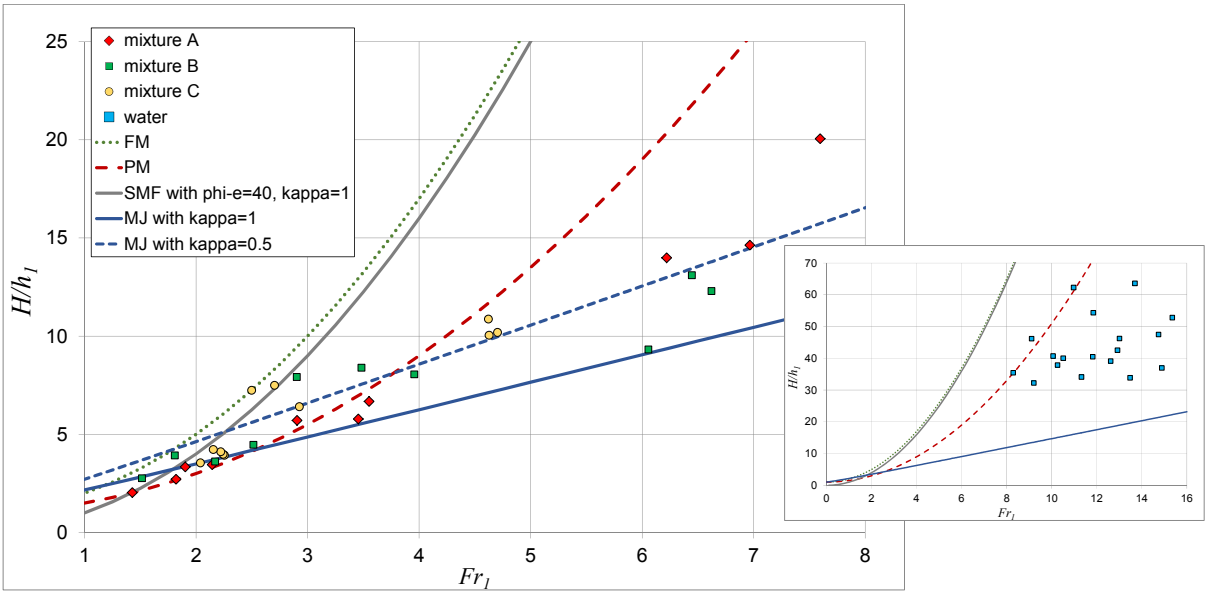

Fig. 3. Run-up heights against a vertical wall (adverse slope of 90°), comparison of experimental results with theoretical models. For the FM, SMF and MJ models equal densities $\rho_1 = \rho_2$ are assumed before and at the obstacle. The inset shows results for the clear water experiments.

3.3. Discussion

One may argue that run-up on an adverse slope (Fig. 2) is best described by gradual deceleration and smooth transfer of mass and momentum from the body to the flow head, as reflected by the SMF model. Our experimental results indicate that an increasing basal friction angle ϕ_e would be necessary for increasing Froude number or flow velocities to provide a reasonable fit with the SMF model prediction (if we neglect possible discrepancies due to the steady, uniform flow assumption for the analytical models). This may appear to be counterintuitive at first sight (since a "dilatation" effect might be expected for higher granular temperatures) and indicates a possible limitation of the SMF model. If we assume, however, that the friction force in the run-up zone is governed by a velocity-squared dependent, Chezy-like friction term (as in the Voellmy fluid model often used for debris flows), then a resulting increase of the total friction with increasing velocity can be justified (note that the approach flow depths h_1 varied much less in our experiments than the approach flow velocity v_1).

A common observation for both the adverse slope (Fig. 2) and the vertical wall experiments (Fig. 3) is that for an approximate agreement of the experimental data with the MJ model an earth pressure coefficient κ smaller than 1 would be required for Fr_1 values larger than about 2.5 to 2.8, whereas a value $\kappa \approx 1$ appears to be appropriate for smaller Froude numbers. This finding is somewhat counterintuitive, as a larger longitudinal compression of the flow requires larger κ values in the range of passive earth pressure coefficients (Hungr, 1995), and a larger longitudinal compression of the flow may be expected for our debris-flow experiments with higher Froude numbers.

However, it should be kept in mind that the comparison of our run-up heights with the analytical models represents a simplification in view of the unsteady and non-uniform approach flow to the obstacle in the experiments. Iverson et al (2016) found that the SMF model yielded predictions of relative run-up heights that were broadly in agreement with results of more accurate simulations with a numerical model; however, the SMF model yielded relative run-up heights that were generally too small if $Fr_1 = 1$ and too large if $Fr_1 = 5$, while they were more accurate if $Fr_1 = 3$. For our experiments with an adverse slope of 30° as obstacle, there is a qualitatively somewhat similar comparison in the sense that the SMF model (with $\kappa = 1$) underestimates the data for smaller Fr_1 and overestimates for larger Fr_1 values.

It is somewhat surprising that MJ model is not in agreement with the clear water experiments for the vertical wall case (although the relative disagreement is less than for the adverse slope case). Concerning the other vertical wall experiments (Fig. 3), we observed a qualitative difference in the run-up behavior depending on flow velocity (or Froude number). For smaller Fr_1 values, sediment tended to pile up in form of a ramp in front of the obstacle, which helped redirect some incoming flow momentum upward. This tendency was more pronounced for the coarser

mixtures B and C that promoted the formation of static deposits, and this could partially explain why these mixtures lead to higher run-up measurements than mixture A, for Froude numbers smaller than about 4. This piling up of sediments in front of the obstacle producing a ramp may also be a reason why the SMF model (with $\phi_e = 40°$ and $\kappa = 1$) may reasonably well describe the debris flow experiments lower Fr_1 numbers (1 to 3). This piling up of sediments in front of the obstacle producing a ramp also occurred for the adverse slope experiments for smaller Froude numbers. For the adverse slope experiments and larger Froude numbers, deflection of flow when encountering the obstacle was observed.

An important limitation of our study is the fact that our experiments involved a very small scale compared to natural events. According to Iverson (2015), miniaturized debris flows exhibit disproportionately large effects of viscous shear resistance and cohesion as well as disproportionately small effects of excess pore-fluid pressure that is generated by debris dilation or contraction.

4. Conclusions

While run-up on an adverse slope is best described by gradual deceleration and smooth transfer of mass and momentum from the body to the flow head, run-up against a vertical barrier is dominated by an abrupt and complete stoppage of the incoming flow. This leads to a rapid upward jump in the surface elevation of the approach flow, and to a shock wave travelling upstream. The experimental results reveal that the run-up mechanism is strongly dependent on incoming flow conditions. Supercritical watery flows resulted in a vertical jet mechanism, granular dry flows resulted in a pile-up mechanism instead of a distinct run-up. The observed run-up heights were generally within the range predicted by the theoretical models, but none of them appears to be universally applicable to the entire range of investigated flow conditions. The commonly used energy principle is not always a conservative method to estimate run-up heights.

References

Choi, C.E., Au-Yeung, S.C.H., Ng, C.W.W., and Song, D., 2015, Flume investigation of landslide granular debris and water runup mechanisms: Géotechnique Letters, v. 5, p. 28–32, doi:10.1680/geolett.14.00080.

Kwan, J.S.H., 2012, Supplementary Technical Guidance on Design of Rigid Debris-resisting Barriers: GEO Report No. 270, Geotechnical Engineering Office, Hong Kong, https://www.cedd.gov.hk/eng/publications/geo_reports/doc/er270/er270links.pdf.

Hákonardóttir, K. M., Hogg, A., and Jóhannesson, T., 2003, A laboratory study of the interaction between supercritical, shallow flows and dams: Icelandic Meteorological Office, Vedurstofa Islands, http://www.vedur.is/media/vedurstofan/utgafa/greinargerdir/2003/03038.pdf.

Hungr, O., 1995, A model for the runout analysis of rapid flow slides, debris flows, and avalanches: Canadian Geotechnical Journal, v. 32, p. 610–623, doi:10.1139/t95-063.

Mancarella, D., and Hungr, O., 2010, Analysis of run-up of granular avalanches against steep, adverse slopes and protective barriers: Canadian Geotechnical Journal, v. 47, p. 827–841, doi: 10.1139/T09-143.

Iverson, R.M., 2015, Scaling and design of landslide and debris-flow experiments: Geomorphology, v. 244, p. 9–20, doi:10.1016/j.geomorph.2015.02.033.

Iverson, R.M., George, D.L., and Logan, M., 2016, Debris flow runup on vertical barriers and adverse slopes: Journal of Geophysical Research, Earth Surface, v. 121, p. 2333–2357, doi:10.1002/2016JF003933.

Jóhannesson, T., Gauer, P., Issler, P., Lied, K. (eds.) 2009, The design of avalanche protection dams: recent practical and theoretical developments: European Commission Directorate for Research, Brussells, Project Report EUR 2339, http://www.preventionweb.net/files/10851_avalancheprotection.pdf.

Scheidl, C., Chiari, M., Kaitna, R., Müllegger, M., Krawtschuk, A., Zimmermann, T., and Proske, D., 2013, Analysing debris-flow impact models, based on a small scale modelling approach: Surveys in Geophysics, v. 34, p. 121–140, doi:10.1007/s10712-012-9199-6.

Scheidl, C., McArdell, B.W., and Rickenmann, D., 2015, Debris-flow velocities and superelevation in a curved laboratory channel: Canadian Geotechnical Journal, v. 52, p. 305–317. doi:10.1139/cgj-2014-0081.

Takahashi, T., and Yoshida, H., 1979, Study on the deposition of debris flows, Part 1—Deposition due to abrupt change of the bed slope [in Japanese with English abstract]: Annals of the Disaster Prevention Research Institute, Kyoto Univ., Japan, 22 B-2.